F. Gómez-Cuba and M. Zorzi, "Twice Simulated Annealing Resource Allocation for mmWave Multi-hop Networks with Interference.," *ICC 2020 - 2020 IEEE International Conference on Communications (ICC)*, 2020, pp. 1-7

DOI: 10.1109/ICC40277.2020.9149128

# Twice Simulated Annealing Resource Allocation for mmWave Multi-hop Networks with Interference.

Felipe Gómez-Cuba† and Michele Zorzi
Dept. of Information Engineering, University of Padova, Italy
Email: gomezcuba@gts.uvigo.es zorzi@dei.unipd.it

***Abstract*—This paper proposes link scheduling and power allocation algorithms for mmWave picocellular integrated access and backhaul networks. The proposed algorithm does not assume that interference is negligible and takes it into account in the solution. The algorithm supports any state of the art multi-user MIMO and hybrid beamforming schemes at the physical layer. The link scheduling and power allocation subproblems are solved using two separate simulated annealing (SA) algorithms which can also be individually combined with other pre-existing sub-optimal algorithms for the other subproblem. Particularly, mixed-integer linear programming for fixed power link scheduling, which is optimal in a special interference-free case, is shown to perform much worse than the proposed algorithm. SA link scheduling with water-filling power allocation performs close to the optimal, while reducing power allocation complexity.**

***Index Terms*—millimeter wave, multi-hop, power allocation, scheduling**

## I. Introduction

Recent updates in cellular [1] and WLAN [2] standards have introduced support for mmWave frequencies ($30-300$ GHz) where wider, less crowded bands can contribute to alleviate spectrum scarcity. However at these frequencies the pathloss, absorption and blockage are more severe [3], [4]. Although the reduced wavelength permits to pack many antenna elements given a fixed circuit area, it is expected that mmWave transmissions display a more limited range than conventional frequencies. For this reason, Integrated Access and Backhaul (IAB) multi-hop picocellular architectures are considered in order to alleviate deployment costs [5], [6]. Figure 2 illustrates such multi-hop picocellular architecture, featuring some wired-backhaul APs, called Base Stations (BS), which provide wireless backhaul links to the remaining APs, named Relay Nodes (RN), using the same radio interfaces that are used to serve the User Equipment (UE) terminals.

MmWave bands show differences with sub-6 GHz systems. Since pathloss is severe, only highly directive transmissions with large array dimensions can reach the destination, i.e., massive Multiple Input Multiple Output (MIMO) is imperative. Moreover, high bandwidth Analog to Digital Converters (ADC) consume a lot of power, thus we cannot digitize each antenna signal independently, and Hybrid analog-digital Beamforming (HBF) radio architectures as in Fig. 1 are employed instead [7]. Thirdly, typical mmWave channel matrices are rank-deficient, meaning that their largest eigenvalue accounts for most of the transferred energy [3], [4]. As a result, Space Division Multiplexing (SDM) used by the same transmitter and receiver pair produces negligible benefits. Still, we can use Multi-User MIMO (MU-MIMO) schemes [8] to leverage significant spatial multiplexing gains by scheduling same-transmitter-different-receiver or different-transmitter-same-receiver links simultaneously. In addition, due to the high directivity, some inherent interference avoidance is present, and the medium access does not need to enforce a global separation between downlink (DL) and uplink (UL) phases. 3GPP New Radio (NR) frames have "flexible" slots that can be scheduled as either DL or UL indistinctly by different access points [1], enabling *Dynamic Duplex* scheduling [9].

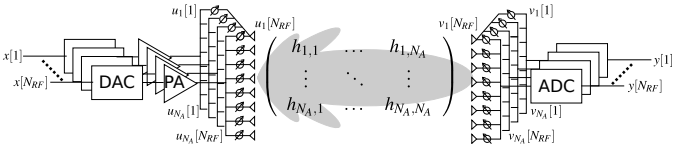


Figure 1. Hybrid analog-digital Beamforming scheme with $N_A$ antennas and $N_{RF}$ RF chains capable of steering $N_{RF}$ simultaneous analog beams.

Some prior works have studied mmWave under the assumption that interference can be ignored. This assumption is often found in multi-hop scheduling research [10]–[12]. Even though this would be justified under perfect link directivity, separate studies on mmWave single-hop cellular systems suggest that this assumption does not always hold [13]. The main contribution of this paper is to study the impact of non-negligible interference on link scheduling and power allocation schemes for mmWave IAB networks with MU-MIMO. We implement a scheduler for the case with interference and compare it with the optimal scheduler for the interference-free case given in [12]. Our solution employs two separate instances of Simulated Annealing (SA) optimization [14], one to select which nodes transmit or receive and another for power allocation. SA is a heuristic that finds near-optimal solutions efficiently. Our numerical simulations show that the baseline scheduler performs significantly worse than the twice-SA near-optimal when there is some interference. In addition, we find that a low complexity practical algorithm can be adopted using our SA link scheduling proposal with water-filling power

†: Gómez-Cuba is now with Univ. of Vigo, Spain. This project has received funding from the European Union's Horizon 2020 research and innovation programme under the Marie Skłodowska-Curie grant agreement No 704837.

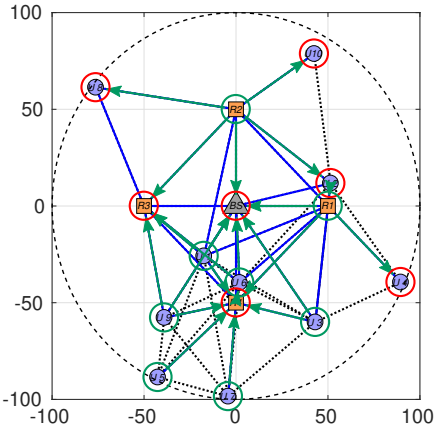

Figure 2. Illustration of IAB picocell with 4 RNs.

allocation, which improves significantly on the baseline and performs close to the twice-SA near-optimal.

The rest of this paper is structured as follows. Section II defines the scheduling system model. Section III describes the physical layer beamforming model. Section IV describes the SA link selection algorithm. Section V describes the SA power allocation algorithm. Section VI discusses extensive numerical simulations. Finally Section VII summarizes the conclusions and future work.

## II. System Model

We assume a mmWave IAB network formed by Base Stations (BS), Relay Nodes (RN) and User Equipments (UEs). Not all pairs of devices form feasible links. We represent this as a graph $\mathcal{G}(\mathcal{N},\mathcal{L})$, where $n \in \mathcal{N}$ is the set of nodes and $(n,m) \triangleq \ell \in \mathcal{L}$, with $n,m \in \mathcal{N}$, is the set of *feasible* links, that may or may not be active simultaneously. The scheduler selects a subset of *active* links $\mathcal{B}(t) \subset \mathcal{L}$ corresponding to the simultaneous transmissions at different time instants $t$. For example, in Fig. 2 the blue lines represent feasible inactive links, and the green arrows represent active links. The links are unidirectional, $(n,m) \neq (m,n)$, but feasibility is reciprocal ($(n,m) \in \mathcal{L} \Leftrightarrow (m,n) \in \mathcal{L}$). For each node $n$ we denote its set of adjacent nodes as $\mathcal{A}(n)$. The UEs and RNs support multi-attachment and have a pair of available links with all APs in their range. All nodes have MU-MIMO HBF radios with a sufficient number of RF chains to communicate with all their neighbors simultaneously, $N_{RF}(n) \geq |\mathcal{A}(n)|$. UE-UE pairs (dashed black lines in Fig. 2) are not feasible and not reflected in $\mathcal{A}(n)$, but can represent interference.

For the sake of readability we will describe the model assuming that BSs, RNs and UEs have the same transmit power limit $P$, receiver noise power $N_o$, number of antennas $N_A$ and number of RF chains $N_{RF}$. We remark that this is merely for clarity and is not a limitation of our approach. Introducing variable values for these parameters in each of the nodes in our model is a trivial extension.

For each node $n \in \mathcal{N}$ we denote its transmitting-state binary variable $s_n(t)$, which is one if node $n$ transmits at instant $t$ and zero otherwise. We assume that all nodes have half-duplex MU-MIMO radios, capable of multiple simultaneous transmissions or multiple simultanous receptions, but no simultaneous transmission and reception. Hence, for each pair $(n,m) \in \mathcal{L}$ we denote the link-active binary variable $b_{n,m}(t) = s_n(t)(1-s_m(t))$. For example, in Fig. 2 the transmitting nodes are highlighted with a green circle, and the receiving nodes with a red circle. It can be noted that multiple active transmissions (green arrows) may come out of some transmitters or go into some of the receivers. Finally, when multiple transmissions are performed simultaneously, each node $n$ divides its total available power $P$ among all its active links, transmitting on each a fraction of its available power denoted by $p_{n,m}(t)P$, where the normalized power fractions $p_{n,m}(t)$ satisfy $\sum_{m\in\mathcal{A}(n)} p_{n,m}(t) \leq 1$ for the total power budget and $p_{n,m}(t) \leq s_n(t)$ for the half-duplex constraint.

We assume that time is divided in frames and the scheduler makes frame-by-frame decisions. For this, the upper layers interface with the scheduler by providing a list of weights that assign a certain value to the delivery of one bit through each link, denoted $w_{n,m}(t)$. This framework permits embedding our scheduler into a wide variety of well-known networking, congestion control, routing and quality of service algorithms for multi-hop networks, such as for example [12]. Due to the fact that at each time $t$ the scheduler makes decisions based only on $w_{n,m}(t)$, in the rest of the paper we will drop the time index indication $(t)$ from our notation.

We denote $N = |\mathcal{N}|$ and $L = |\mathcal{L}|$. Finally, we stack all the state variables in a vector $\mathbf{s} = (s_1 \dots s_N)^T \in \{0,1\}^N$. A change in the state leads to changes in the half-duplex constraint on power allocation. We stack all the power allocation variables in $\mathbf{p} = (p_1 \dots p_L)^T \in (\mathbb{R}^+)^L$. We define the set of all $\mathbf{p}$ which are valid when the state is $\mathbf{s}$ as

$$\mathcal{P}(\mathbf{s}) = \{\mathbf{p} : \sum_{m\in\mathcal{A}(n)} p_{n,m} \leq 1 \cap p_{n,m} \leq s_n \forall n,m\},$$

and the set of all valid power allocations is $\mathcal{P} = \bigcup_{\mathbf{s}} \mathcal{P}(\mathbf{s})$.

Using the above, we define the Signal to Interference Plus Noise Ratio (SINR) of link $n,m$ given $\mathbf{p}$ as

$$\gamma_{n,m}(\mathbf{p}) = \frac{|\mathbf{v}_{n,m}^H \mathbf{H}_{n,m} \mathbf{u}_{n,m}|^2 p_{n,m} P}{\sum_{\substack{(i,j)\in\mathcal{N}^2 \\ (i,j)\neq(n,m)}} |\mathbf{v}_{n,m}^H \mathbf{H}_{i,m} \mathbf{u}_{i,j}|^2 p_{i,j} P + N_o} \quad (1)$$

where $\mathbf{H}_{n,m}$ is the $N_A \times N_A$ MIMO channel matrix between nodes $n$ and $m$, $\mathbf{u}_{n,m}$ is the transmission-beamforming vector applied by node $n$ to its transmission towards $m$, and $\mathbf{v}_{n,m}$ is the reception-beamforming vector applied by node $m$ when receiving from $n$. In the denominator, $|\mathbf{v}_{n,m}^H \mathbf{H}_{i,m} \mathbf{u}_{i,j}|^2$ represents an interfering signal with mismatched vectors, i.e., transmitted from $i$ to $j$, but crossing the channel for the pair $(i,m)$ and captured at $m$ with the vector $\mathbf{v}_{n,m}$. Note that the interference takes into account all pairs of nodes $(i,j) \in \mathcal{N}^2$, not only those which are valid links and satisfy $j \in \mathcal{A}(i)$. Particularly, there can be UE-UE interference despite the fact that UE-UE links are not feasible. For example, in Fig. 2 the pairs of nodes that cannot form a link but produce

interference are depicted with dotted black lines. Moreover, our scheduling model is compatible with multiple models for the distribution of $\mathbf{H}_{n,m}$ and techniques for the design of the beamforming vectors $\mathbf{v}_{n,m}$, $\mathbf{u}_{n,m}$. In Section III we provide a full description of the approach used in our simulations.

Using the definition of the SINR the frame-by-frame maximum sum-rate-value scheduling problem is defined as follows

$$\max_{\mathbf{s}\in\{0,1\}^N} \max_{\mathbf{p}\in\mathcal{P}(\mathbf{s})} \sum_{\substack{n\in\mathcal{N}\\ m\in\mathcal{A}(n)}} b_{n,m} w_{n,m} \log_2(1+\gamma_{n,m}(\mathbf{p})). \quad (2)$$

In this paper we study the solution to (2), which optimizes both $\mathbf{s}$ and $\mathbf{p}$ taking into account their dependence via $\mathcal{P}(\mathbf{s})$ and the dependence of different nodes due to the interference.

In addition, two easier related problems may be defined. First, let us denote the SNR of link $(n,m)$ as

$$\frac{|\mathbf{v}_{n,m}^H \mathbf{H}_{n,m} \mathbf{u}_{n,m}|^2 P}{N_o} . p_{n,m} \triangleq \overline{\gamma}_{n,m} p_{n,m} \quad (3)$$

Replacing the SINR by the SNR in (2) leads to the following maximum interference-free sum-rate-value problem

$$\max_{\mathbf{s}\in\{0,1\}^N} \max_{\mathbf{p}\in\mathcal{P}(\mathbf{s})} \sum_{\substack{n\in\mathcal{N}\\ m\in\mathcal{A}(n)}} b_{n,m} w_{n,m} \log_2(1+\overline{\gamma}_{n,m} p_{n,m}), \quad (4)$$

where one possible interpretation of existing schedulers for mmWave systems assuming negligible interference such as [10]–[12] is that they implicitly claim that the solution of (4) is identical or close enough to the solution of (2).

Secondly, let us assume that power allocation may follow some arbitrary scheme that is not motivated by (2). Let us denote any arbitrary power allocation scheme as a function of $\mathbf{s}$ by $\mathbf{p} = \rho(\mathbf{s})$. Then the maximum sum-rate-value scheduling problem with a given power allocation method $\rho(\mathbf{s})$ is

$$\max_{\mathbf{s}\in\{0,1\}^N} \sum_{\substack{n\in\mathcal{N}\\ m\in\mathcal{A}(n)}} b_{n,m} w_{n,m} \log_2(1+\gamma_{n,m}(\rho(\mathbf{s}))). \quad (5)$$

An interference-free variant of this problem may be defined by substituting the SINR with the SNR $\overline{\gamma}_{n,m}\rho(\mathbf{s})_{n,m}$.

We will consider the following power allocation schemes:

- Fixed Power (FP): We assume that each RF chain in the transmitter has an independent power amplifier, and that $|\mathcal{A}(n)| \leq N_{RF} \forall n$. Thus the transmitted power is a constant value $\rho_{FP}(\mathbf{s})_{n,m} = s_n/N_{RF}$.
- Split Power (SP): Power is split equally among the *active* RF chains $\rho_{SP}(\mathbf{s})_{n,m} = \frac{s_n}{\sum_{m\in\mathcal{A}(n)} b_{n,m}}$.
- Water-Filling (WF): Due to the lack of interference, in (4) the optimal power allocation uses a weighted water-filling algorithm, that is, $\rho_{WF}(\mathbf{s})_{n,m} = w_{n,m}\max(0, \lambda_n - \frac{w_{n,m}}{b_{n,m}\overline{\gamma}_{n,m}})$ where $\lambda_n$ is a Lagrange multiplier that can be computed from the constraint $\sum_{m\in\mathcal{A}(n)} p_{n,m} \leq 1$.
- Optimal (OP): Solve the inner max. in (2), i.e.,

$$\rho_{OP}(\mathbf{s}) = \arg\max_{\mathbf{p}\in\mathcal{P}(\mathbf{s})} \sum_{\substack{n\in\mathcal{N}\\ m\in\mathcal{A}(n)}} b_{n,m} w_{n,m} \log_2(1+\gamma_{n,m}(\mathbf{p})). \quad (6)$$

Finally, solving (5) using $\rho_{OP}(\mathbf{s})$ solves (2).

## III. Beamforming Design

Typical mmWave channel models adopt an explicit multipath model as a sum of planar waves such as

$$\mathbf{H}_{n,m} = \sqrt{G_{n,m}} \sum_{c\in\mathcal{C}} \sum_{r\in\mathcal{R}(c)} \sqrt{g_c g_r} e^{j\theta_r} \mathbf{a}(\beta_c+\beta_r)\mathbf{a}(\alpha_c+\alpha_r)^H, \quad (7)$$

where $\sqrt{G_{n,m}}$ is the macroscopic pathloss between $n$ and $m$. The set $\mathcal{C}$ is a collection of "clusters" of multipath rays, and $\mathcal{R}(c)$ is the set of rays of each cluster $c$. For each cluster and ray, $g_c$ is a common propagation gain term to all rays in cluster $c$, and $g_r$ the differential gain of each ray. Likewise $\theta_r$ is the phase of the ray, and $\alpha_c + \alpha_r$ and $\beta_c + \beta_r$ the cluster and ray angles of departure from the transmitter array and arrival to the receive array, respectively. $\mathbf{a}(\alpha)$ is a vector that models each array element as a function of the angle of departure/arrival $\alpha$. For example, in uniform linear arrays (ULA) it is

$$\mathbf{a}(\alpha) = \frac{1}{\sqrt{N_A}} \left(1, e^{-j\pi\sin(\alpha)} \dots e^{-j\pi(N_A-1)\sin(\alpha)}\right)^T. \quad (8)$$

The normalization $\sum_{c,r} g_c g_r = 1$ means that $\|\mathbf{H}_{n,m}\|^2 = G_{n,m}$. Typically the cluster common angles vary much more than the intra-cluster angular differences, and thus all rays in a cluster come from similar directions. Moreover, $|\mathcal{C}| \ll N_A$ and the $g_c g_r$'s have a large variance, and thus $\mathbf{H}_{n,m}$ is rank deficient and its largest singular value accounts for almost all the magnitude of $\|\mathbf{H}_{n,m}\|^2$. Typical mmWave HBF schemes exploit this directivity and rank deficiency.

When $N_A \gg N_{RF}$, the overhead of fully estimating $\mathbf{H}_{n,m}$ is prohibitive, and HBF vectors are selected from "beamforming codebook" sets that we denote $\mathcal{U}$, $\mathcal{V}$. The transmitter sends separate control reference signals using each element of $\hat{\mathbf{u}} \in \mathcal{U}$, and the receiver attempts to detect the reference signals using each element in $\hat{\mathbf{v}} \in \mathcal{V}$. A preferred pair $(\hat{\mathbf{u}}^*, \hat{\mathbf{v}}^*)$ is thus identified, and the receiver only needs to feed back the index that $\hat{\mathbf{u}}^*$ occupies in the look-up table $\mathcal{U}$.

In our simulations we adopt the ULA array model. By generating a codebook of $N_A$ vectors using $\mathbf{a}()$ at certain angles, $\mathcal{U}_{DFT} = \mathcal{V}_{DFT} = \{\mathbf{a}(\sin^{-1}(\frac{2n}{N_A} - 1)) : n \in \{0 \dots N_A - 1\}\}$, then $\mathcal{U}_{DFT}$ conveniently becomes the set of columns of an $N_A$-DFT matrix. For this reason $\sin(\alpha)$ in (8) is called the "spatial frequency". The DFT codebook is convenient as it can be implemented with fully analog phase-arrays or with lensed arrays. Figure 3 illustrates $\mathcal{U}_{DFT}$ for $N_A = 8$.

We will compare two techniques. First, a minimal feedback scheme using only codebook look-up. Secondly, a low overhead Minimum Mean Squared Error (MMSE) refinement.

### A. Minimal feedback Beamforming

We assume that the preferred pair $(\hat{\mathbf{u}}^*, \hat{\mathbf{v}}^*)$ is selected as the elements of $\mathcal{U}_{DFT}$ and $\mathcal{V}_{DFT}$ with the strongest detected reference signal, $(\hat{\mathbf{u}}^*, \hat{\mathbf{v}}^*) = \arg\max_{(\hat{\mathbf{u}},\hat{\mathbf{v}})\in\mathcal{U}_{DFT}\times\mathcal{V}_{DFT}} |\hat{\mathbf{v}}^H \mathbf{H}_{n,m} \hat{\mathbf{u}}|^2$.

There is no overhead beyond this coarse directional neighbor detection. The beamforming vectors are $\mathbf{u}_{n,m} = \hat{\mathbf{u}}^*$ and $\mathbf{v}_{n,m} = \hat{\mathbf{v}}^*$, which maximize the SNR (3) and are optimal for interference-free scheduling (4).

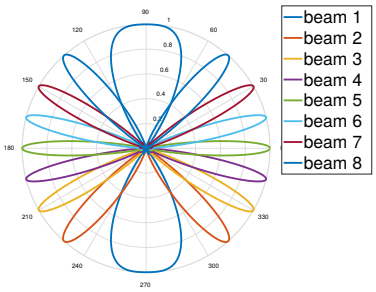


Figure 3. Beam patterns for $\mathcal{U}_{DFT}$ with $N_A = 8$.

### B. Low overhead MMSE refinement

We adopt the MMSE method because when $P/N_o$ is low it behaves like a matched filter, maximizing the SNR, and when it is high it behaves as the ZF combiner, maximizing the SIR. Thus MMSE offers good SINR behavior in all regimes.

We begin with the pair $(\hat{\mathbf{u}}^*, \hat{\mathbf{v}}^*)$ acquired during neighbor detection. For each state $\mathbf{s}$ we let the receivers modify $\mathbf{v}_{n,m}$ in order to improve the SINR, whereas we still fix $\mathbf{u}_{n,m} = \mathbf{u}^*$. Given $\mathbf{s}$, each receiver $m$ is set to receive from the set of transmitters $\mathcal{T}_m(\mathbf{s}) = \{n : s_n = 1, m \in \mathcal{A}(n)\}$. In the refinement we assume that an additional low dimensional MIMO channel estimation pilot can be transmitted. All transmitters send scalar training signals using $\mathbf{u}_{n,m} = \mathbf{u}^*$ as beamforming vector, and the receivers place each of the preliminary vectors $\hat{\mathbf{v}}_n^*$ corresponding to each transmitter $n \in \mathcal{T}_m(\mathbf{s})$ in one of their $N_T \leq N_{RF}$ RF chains. Thus, the following equivalent low dimensional $N_T \times N_T$ MIMO matrix is obtained

$$\mathbf{H}_m^{eq}(\mathbf{s}) = \begin{pmatrix} \mathbf{v}_1^{*H}\mathbf{H}_{1,m}\mathbf{u}_{1,m} & \dots & \mathbf{v}_1^{*H}\mathbf{H}_{N_T,m}\mathbf{u}_{N_T,m} \\ \vdots & \ddots & \vdots \\ \mathbf{v}_{N_T}^{*H}\mathbf{H}_{1,m}\mathbf{u}_{1,m} & \dots & \mathbf{v}_{N_T}^{*H}\mathbf{H}_{N_T,m}\mathbf{u}_{N_T,m} \end{pmatrix}. \tag{9}$$

Finally the receiver designs the MMSE post-combiner

$$\mathbf{V}_m^{MMSE}(\mathbf{s}) = \left(\mathbf{H}_m^{eq}(\mathbf{s})^H\mathbf{H}_m^{eq}(\mathbf{s}) + \frac{N_o}{P}\mathbf{I}_{N_T}\right)^{-1}\mathbf{H}_m^{eq}(\mathbf{s})^H, \tag{10}$$

and the effective HBF receive-beamforming vectors become

$$(\mathbf{v}_{1,m} \dots \mathbf{v}_{N_T,m}) = \frac{\mathbf{V}_m^{MMSE}(\mathbf{s})}{\sqrt{\|\mathbf{V}_m^{MMSE}(\mathbf{s})\|^2}}(\mathbf{v}_1^* \dots \mathbf{v}_{N_T}^*). \tag{11}$$

## IV. State allocation Design

SA is a heuristic inspired by "annealing" in materials whose molecular structure can be in different states that correspond to points in an energy function. By heating the material, its state moves randomly around the energy function. When the material cools down, it enters states of lower energy. Provided that the cooling is slow compared to the random state change, the global minimum can be achieved [14] (Fig. 4).

The general SA algorithm in Alg. 1 is applicable to multiple problems by a careful design of the function

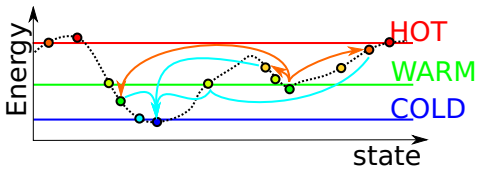


Figure 4. Illustration of annealing in a material: when heated, the state goes from one or several local minimum(s) to random points. During a slow cooldown, all random state paths converge to the global minimum.

**Algorithm 1** Simulated Annealing

**Inputs:** minimization target function $f(\mathbf{x})$, initial state $\mathbf{x}_o$, no. stages $n_s$, no. random points $n_p$, initial climb probability $P_o$, final climb probability $P_f$
Set current state $\mathbf{x}_c = \mathbf{x}_o$ with energy $E_c = f(\mathbf{x}_c)$,
Initialize at high temperature $T = -1.0/\log(P_o)$
Initialize $\Delta_{avg} = 0$, $n_{accepted} = 1$
**for** stage from 1 to $n_s$ **do**
  **for** random point from 1 to $n_p$ **do**
    Generate $\mathbf{x}_a = \texttt{random\_change}(\mathbf{x}_c)$
    **if** $(f(\mathbf{x}_a) < E_c)$ or (with prob. $e^{\frac{-|f(\mathbf{x}_a)-E_c|}{\Delta_{avg}T}}$) **then**
      $\mathbf{x}_c = \mathbf{x}_a$
      $n_{accepted} = n_{accepted} + 1$
      $\Delta_{avg} = \Delta_{avg}\frac{n_{accepted}-1}{n_{accepted}} + \frac{|f(\mathbf{x}_a)-E_c|}{n_{accepted}}$
    **end if**
  **end for**
  Lower temperature $T = T\left(\frac{\log(P_o)}{\log(P_f)}\right)^{\frac{1}{n_s-1}}$
**end for**
**Output:** $\mathbf{x}_c$

$\texttt{random\_change}(\mathbf{x}_c)$. The algorithm imitates physical annealing by selecting random points in the energy function. If the new point has lower energy, the algorithm always selects it. If the new point has higher energy, it is only selected with a probability that depends on the temperature. In Alg. 1 the "cooldown" is implemented in $n_s$ stages, where a sufficient number of random points $n_p$ must be generated for each stage. However, if $n_s n_p$ is too high, scheduling computation may take too much time compared to the mobile UE speeds.

We implement an instance of Alg. 1 to solve (5) given function $\rho(\mathbf{s})$, which we denote SA-s. For this, the optimization variable is the node state vector $\mathbf{x} \equiv \mathbf{s}$ and the negative of the minimization target function is the sum-rate-utility $-f(\mathbf{x}) \equiv (5)$. The initial search point $\mathbf{s}_o$ is a size-$N$ vector of i.i.d. Bernoulli$(0.5)$ values. The key challenge is the definition of the function $\mathbf{s}_a = \texttt{random\_change}(\mathbf{s}_c)$ in Alg. 2. The permutation function must be able to cover the entire space of valid solutions over paths of successive small random perturbations. Preferably, it should produce paths with a uniform probability of visiting any point in the solution space. Since $\mathbf{s} \in \{0,1\}^N$ is an unconstrained size-$N$ binary vector, one possible approach would be to flip one random bit at a time. Another possible approach would be to generate completely i.i.d. Bernoulli vectors each time. We adopted an

**Algorithm 2** State Allocation $\mathbf{s}_a = \texttt{random\_change}(\mathbf{s}_c)$

1: **Input:** binary vector $\mathbf{s}_c$, mean Hamming distance $\lambda$
2: Generate $n_b \sim \min(N, 1 + \text{Poisson}(\lambda - 1))$
3: Generate $\mathbf{s}_{change} \sim \text{RandomPermutation}((\mathbf{1}_{n_b}; \mathbf{0}_{N-n_b}))$
4: **Output:** $\mathbf{s}_a = \mathbf{s}_c$ xor $\mathbf{s}_{change}$

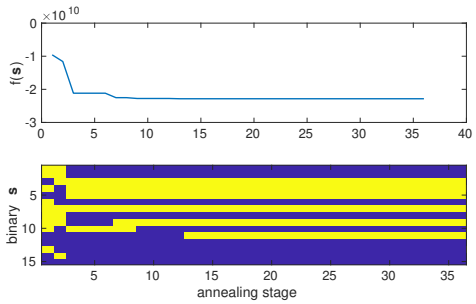


Figure 5. Example run of the SA-$\mathbf{s}$ algorithm with change function Alg. 2.

intermediate approach with a tuning parameter by generating a random number of Poisson arrivals $n_b$ with mean $\lambda$. Thus, $\lambda$ characterizes the mean Hamming distance between the original and generated vectors. Then we select a random subset of $n_b$ coefficients of $\mathbf{s}$ and flip their value. For symmetry, we perform this using a random permutation and xor operation, so that all coefficients of $\mathbf{s}$ are treated equally.

An example demonstration of the behavior of the SA algorithm for state allocation (SA-$\mathbf{s}$) is given in Fig. 5. In this algorithm the SA-$\mathbf{s}$ algorithm selected the schedule shown in Fig. 2 under minimal feedback beamforming with interference as in Sec. III-A and with optimal power allocation (6).

## V. Power allocation Design

We implement a second instance of the SA Alg. 1 to solve the optimal power allocation problem (6) where $\mathbf{s}$ is an input, which we denote SA-$\mathbf{p}$. To reduce the dimensionality, the optimization variables are the power allocation coefficients $\mathbf{x}_c \equiv \hat{\mathbf{p}} = \{p_{n,m} \text{ s.t. } s_n = 1, s_m = 0\}$, a subvector of $\mathbf{p}$, and the other coefficients of $\mathbf{p}$ are fixed to zero. $\mathbf{p} \in \mathcal{P}(\mathbf{s})$ is a region enclosed by a collection of planes defined by the linear constraints $\sum_{m \in \mathcal{A}(n), s_m = 0} p_{n,m} \leq 1 \; \forall n$ and $p_{n,m} > 0 \; \forall n, m$. The negative of the minimization target function is the sum-rate-utility $-f(\mathbf{x}) \equiv (6)$. The initial search point $\hat{\mathbf{p}}_o$ was set to $0.99\rho_{WF}(\mathbf{s})$, since we expect the optimal solution to be similar to WF when the interference is weak. The .99 factor is simply a protection to ensure that the initial point is fully contained inside the validity region and not on its border.

To design $\hat{\mathbf{p}}_a = \texttt{random\_change}(\hat{\mathbf{p}}_c)$ let us denote the set of all transmitters by $\mathcal{T} = \{n \in \mathcal{N} : s_n = 1\}$, and the set of all active links by $\mathcal{B} = \{(n,m) = \ell \in \mathcal{L} : b_{n,m} = 1\}$. We define the $|\mathcal{T}| \times |\mathcal{B}|$ matrix $\mathbf{M}$, where $M_{i,j} = 1$ if $n$ is the $i$-th element in $\mathcal{T}$, $\ell$ is the $j$-th element in $\mathcal{B}$, and $n$ is the transmitter of link $\ell$; and zero otherwise. All the linear constraints can thus be written as

$$\mathbf{M}_2 \hat{\mathbf{p}} \triangleq \begin{pmatrix} \mathbf{M} \\ -\mathbf{I}_{|\mathcal{B}|} \end{pmatrix} \hat{\mathbf{p}} \preceq \begin{pmatrix} \mathbf{1}_{|\mathcal{T}|} \\ \mathbf{0}_{|\mathcal{B}|} \end{pmatrix} \triangleq \mathbf{v}_1, \qquad (12)$$

**Algorithm 3** Power Allocation $\hat{\mathbf{p}}_a = \texttt{random\_change}(\hat{\mathbf{p}}_c)$

1: **Input:** real vector $\hat{\mathbf{p}}_c$, matrix $\mathbf{M}_2$, vector $\mathbf{v}_1$
2: Generate isotropic unit vector $\mathbf{u} \sim |\mathcal{B}|$-SphereUniform
3: Intersection along $\mathbf{u}$ with each of the planes

$$\mathbf{v}_2 \triangleq \mathbf{M}_2 \hat{\mathbf{p}}_c, \quad \mathbf{v}_3 \triangleq \mathbf{M}_2 \mathbf{u}$$

$$\Delta[i] = (v_1[i] - v_2[i])/v_3[i]$$

4: Compute the displacement limits

$$\mu_{\max} = \inf\{\Delta[i] : \Delta[i] > 0\}$$

$$\mu_{\min} = \sup\{\Delta[i] : \Delta(i) < 0\}$$

5: Select uniformly along the segment $\mu \sim U(\mu_{\min}, \mu_{\max})$
6: **Output:** $\hat{\mathbf{p}}_a = \hat{\mathbf{p}}_c + \mu \mathbf{u}$

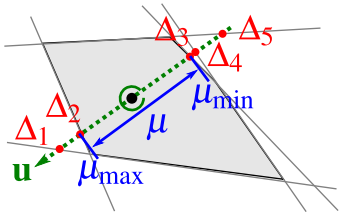


Figure 6. An illustration of Alg. 3.

where $\mathbf{M}_2$ and $\mathbf{v}_1$ give a compact notation that fully represents all linear constraints. Using these definitions, we can define a uniform random perturbation of $\hat{\mathbf{p}}_c$ as in Alg. 3. This is implemented in the 4 steps depicted in Fig. 6: firstly, we select a random movement direction, represented by a unit vector $\mathbf{u}$, uniformly from the $|\mathcal{B}|$-dimensional unit sphere. Secondly, we follow this random direction until we collide with *any* of the planes that define the linear constraints. Thirdly, we identify the segment comprised between the first collisions along the positive and negative directions following $\mathbf{u}$. All points of this segment satisfy all the constraints, so we pick one uniformly.

An example of the SA-$\mathbf{p}$ scheme is given in Fig. 7 for a simple two user broadcast channel with target function

$$f(p_1, p_2) = -\log_2(1 + \frac{p_1}{.04p_2 + 1}) - \log_2(1 + \frac{2p_2}{.08p_1 + 1}).$$

This figure shows that SA-$\mathbf{p}$ follows a path of points $(p_1, p_2)$ formed by random segments contained in the triangle delimited by $p_1 > 0$, $p_2 > 0$ and $p_1 + p_2 \leq 1$. This random path loosely climbs towards a near optimal power allocation. Although not depicted, the main difference with a gradient is that SA-$\mathbf{p}$'s random movement can handle well the non-convexity of the equivalent problem in a larger network.

## VI. Numerical Results

We simulate 1000 random different mmWave picocells networks with 1 BS, 4 RNs located at $90^o$ angles, and 10 UEs with independent uniformly distributed locations in a disc with radius 100 m, such as the example in Fig. 2. For each pair of nodes, we generate the pathloss, the LOS/NLOS/blockage

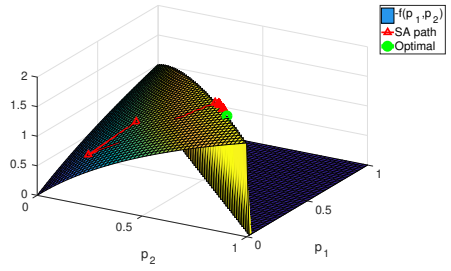


Figure 7. An example run of the SA algorithm for power allocation in a two receiver broadcast channel.

state, and the multipath parameters in (7) using the NYU Wireless mmWave urban microcellular 28 GHz channel model [3]. We select the array dimensions $N_A = 32$ and $N_{RF} = 10$. The radios satisfy $P = 1$ W, $B = 400$ MHz, and $\frac{N_o}{B} = -174$ dB/Hz. The link value weights are generated as $w_{n,m} \sim U(0, 10)$. We set $n_s$ and $n_p$ experimentally as low as possible while the algorithms still performed well, using $n_s = 35$, $n_p = 30$ and $\lambda = 4$ for SA-$\mathbf{s}$; $n_s = 40$ and $n_p = 25$ for SA-$\mathbf{p}$; and $P_o = 1$ and $P_f = 10^{-4}$ for both.

We adopt as a baseline the Mixed Integer Linear Programming (MILP) link selection algorithm from a prior work [12], which is optimal for the interference-free scheduling problem (4) with fixed power allocation $\rho_{FP}(\mathbf{s}) = P/N_{RF}$, but not for (2). The baseline precomputes the "potential capacity" a link would have if selected, which does not depend on $\mathbf{s}$, as

$$c_{n,m} = \log_2(1 + \overline{\gamma}_{n,m} P/N_{RF}),$$

and then rewrites the interference-free fixed-power maximum-sum-rate-utility (4) problem as a linear integer problem:

$$\begin{aligned} &\max_{\mathbf{b}} \sum b_{n,m} w_{n,m} c_{n,m}, \\ &\text{s.t. } b_{n,m} + \frac{1}{|\mathcal{A}(n)|} \sum_{m' \in \mathcal{A}(n)} b_{m',n} \leq 1 \; \forall (n,m). \end{aligned} \tag{13}$$

This type of problem can be solved using standard MILP numerical toolboxes. Both the MILP baseline and the proposed SA algorithms are centralized, and assume the 5G IAB network coexists with a non-standalone 4G control channel.

Fixed power is not always the best power allocation scheme, so we improve the sum-rate-utility by fixing the MILP state allocations, $\mathbf{s}_{MILP}$, and then applying superior power allocation schemes. However, it is not guaranteed that $\mathbf{s}_{MILP}$ is the optimal state vector with the other power allocation schemes. And if there is interference, $\mathbf{s}_{MILP}$ is not guaranteed to be optimal even with fixed power. We proposed SA-$\mathbf{s}$ in Sec. IV to achieve even better performance with any power allocation scheme. Among all combinations of state and power allocation, the twice-SA scheme (SA-$\mathbf{s}$+SA-$\mathbf{p}$) given in Secs. IV and V is a heuristic near the optimal solution of (2).

Unfortunately, the function $\rho_{SA}(\mathbf{s})$ is called $n_s n_a$ times by SA-$\mathbf{s}$. The SA-$\mathbf{s}$+SA-$\mathbf{p}$ algorithm performs $\Theta(n_s^2 n_a^2)$ operations with $n_s$ and $n_a$ around $\sim 30$. This results in millions of evaluations that, even at 1 ns per operation, would accrue a computation time exceeding the 1 ms NR subframe. Still, this algorithm allows to study the ultimate limits of mmWave IAB scheduling, and to identify faster near-optimal algorithms.

In Fig. 8(a) we present the CDF of the achieved sum-rate-value for 1000 networks with an interference-free link model as in (4). In this case the minimal feedback beamforming discussed in Section III-A achieves the optimum SNR. We compare MILP (crosses) vs SA-$\mathbf{s}$ (squares) state allocation for four power allocation methods: FP, SP, WF and SA-$\mathbf{p}$. First, we note that SA-$\mathbf{s}$ scheduling cannot outperform MILP when the power is fixed, as MILP is optimal in this case. In the cases of SP, WF and SA-$\mathbf{p}$, a minor advantage is achieved by SA-$\mathbf{s}$. However, SA-$\mathbf{s}$ offers a very small advantage under the interference-free SNR-only link model (4). Particularly, WF or SA-$\mathbf{p}$ power allocation with SA-$\mathbf{s}$ scheduling do not improve significantly over the much more tractable algorithm combining MILP and WF. Thus, in networks where interference is truly so small that link rates are dominated by the SNR, it would seem that the MILP benchmark is sufficient.

The results change dramatically in Fig. 8(b) where we simulated the same 1000 networks with real interference as in (5). The minimal feedback beamforming in Section III-A is now suboptimal and a relatively strong link interference exists. All algorithms suffer from the interference, but we note that for all four power allocation methods the state allocation using MILP (crosses) performs much worse than using SA-$\mathbf{s}$ (squares). Thus when interference is non-negligible SA-$\mathbf{s}$ finds much better state allocations. Moreover, the gap between MILP-WF and SA-$\mathbf{s}$ with either WF or SP-$\mathbf{p}$ increases. This means that taking into account the non-equal power allocation in the selection of $\mathbf{s}$ offers greater benefits. On the other hand, the performance difference between WF and SA-$\mathbf{p}$ is negligible. We recall that the SA-$\mathbf{s}$+SA-$\mathbf{p}$ scheme is a heuristic near the full fledged optimal solution of (2). The fact that WF and SA-$\mathbf{p}$ perform almost identically suggests that although the interference can in principle influence the optimal power allocation, such influence is very weak. Hence, the main value of our twice-SA algorithm lies in studying this performance gap so we can conclude that SA is necessary in state allocation, but not in power allocation. Thus, practical mmWave picocellular networks can be managed near-optimally using faster WF power allocation provided that the state allocation takes interference into account using SA-$\mathbf{s}$.

Finally we consider whether more sophisticated beamforming can bring the network back into a scenario like the interference free case in Fig. 8(a), or it maintains the behavior of the substantial-interference case in Fig. 8(b). We simulated the same 1000 networks with the low overhead MMSE hybrid beamforming discussed in Section III-B. We note that the performance improves significantly for SA-$\mathbf{s}$ but negligibly for MILP. This is because MILP does not take into accout that $\mathbf{V}_m^{MMSE}(\mathbf{s})$ in (10) depends on $\mathbf{s}$. Thus, regardless of whether we use simple beam selection only or sophisticated hybrid beamforming, mmWave IAB picocellular scheduling needs to take into account the effects of interference for link scheduling. On the other hand, not much is lost by adopting

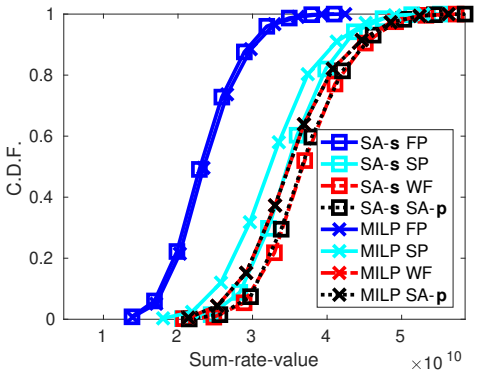


(a) No-interference max-SNR beam selection

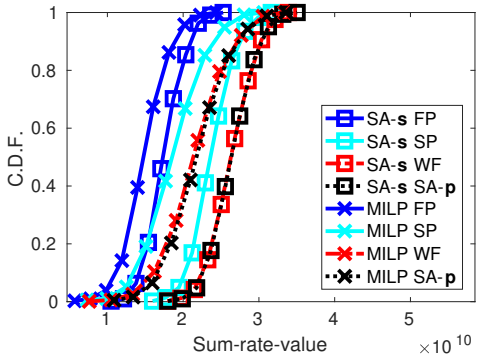


(b) Minimal feedback beam selection with interference

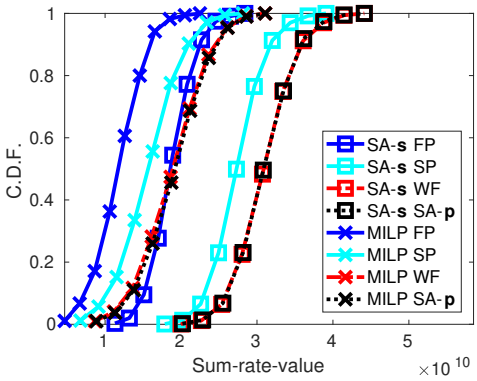


(c) Low overhead MMSE refinement with interference

Figure 8. CDF of total single frame sum-rate-value in 1000 random networks.

the much simpler WF algorithm for power allocation.

## VII. Conclusions and Future Work

In this paper we have derived an optimal link selection and power allocation scheme for mmWave picocellular IAB networks with non-negligible interference. Our solution uses a twice-simulated-annealing approach where nested SA algorithms jointly address the power allocation and transmitter selection problems. We have also discussed suboptimal algorithms of interest in particular cases. Our results show that taking into account interference in the transmitter selection part of the problem can lead to outstanding benefits, whereas taking into account interference in the power allocation does not improve much the result versus traditional water-filling. For this reason, while the two parts of our near-optimal twice-SA algorithm are needed to study the gap between (near) optimal and practical algorithms, only the transmitter selection half should be transferred into practical deployments. This observation remains valid even if sophisticated beamforming is used to partially suppress the interference.

Since our observations stem from the comparison in simulation of near-optimal and sub-optimal algorithms, further study of this gap by analytical methods or in other simulation scenarios should be pursued. Moreover, we leave the study of the optimality gap of SA for future work. In addition, our frame-by-frame scheduling scheme can be integrated into full system level network simulations. Moreover, machine learning schemes can be trained to reproduce the twice-SA near-optimal scheduler to reduce its computational complexity.

## References


[1] 3GPP, "3rd Generation Partnership Project; Technical Specification Group Radio Access Network; NR; NR and NG-RAN Overall Description; Stage 2 (Release 15)," *ETSI TS 38.300*, no. 15.7.0, 2019.

[2] P. Zhou, K. Cheng, X. Han, X. Fang, Y. Fang, R. He, Y. Long, and Y. Liu, "IEEE 802.11ay-Based mmWave WLANs: Design Challenges and Solutions," *IEEE Communications Surveys Tutorials*, vol. 20, no. 3, pp. 1654–1681, 2018.

[3] M. K. Samimi and T. S. Rappaport, "3-D Millimeter-wave statistical channel model for 5G wireless system design," *IEEE Transactions on Microwave Theory and Techniques*, vol. 64, no. 7, pp. 2207–2225, June 2016.

[4] 3GPP, "3rd Generation Partnership Project; Technical Specification Group Radio Access Network; Study on channel model for frequency spectrum above 6 GHz Technical Report (Release 14)," *3GPP TR 38 900*, vol. 14.3.1, pp. 1–87, 2017.

[5] M. Polese, M. Giordani, A. Roy, D. Castor, and M. Zorzi, "Distributed path selection strategies for integrated access and backhaul at mmWaves," in *IEEE Global Communications Conference (GLOBECOM)*, December 2018, pp. 1–7.

[6] M. Polese, M. Giordani, T. Zugno, A. Roy, S. Goyal, D. Castor, and M. Zorzi, "Integrated Access and Backhaul in 5G mmWave Networks: Potentials and Challenges," *IEEE Communications Magazine*, vol. 58, no. 3, March 2020.

[7] K. Venugopal, A. Alkhateeb, N. G. Prelcic, and R. W. Heath, "Channel estimation for hybrid architecture based wideband millimeter wave systems," *IEEE Journal on Selected Areas in Communications*, vol. 35, no. 9, pp. 1996–2009, June 2017.

[8] E. Björnson, E. G. Larsson, and T. L. Marzetta, "Massive MIMO: ten myths and one critical question," *IEEE Communications Magazine*, vol. 54, no. 2, pp. 114–123, February 2016.

[9] B. Yu, S. Mukherjee, H. Ishii, and L. Yang, "Dynamic TDD support in the LTE-B enhanced local area architecture," in *GC'12 Workshop: The 4th IEEE International Workshop on Heterogeneous and Small Cell Networks (HetSNets)*, 2012.

[10] R. Mudumbai, S. Singh, and U. Madhow, "Medium Access Control for 60 GHz Outdoor Mesh Networks with Highly Directional Links," in *IEEE INFOCOM*, April 2009, pp. 2871–2875.

[11] R. Ford, F. Gómez-Cuba, M. Mezzavilla, and S. Rangan, "Dynamic time-domain duplexing for self-backhauled millimeter wave cellular networks," in *IEEE International Conference on Communications (ICC) Workshop on Next Generation Backhaul/Fronthaul Networks (BackNets)*, 2015.

[12] F. Gómez-Cuba and M. Zorzi, "Optimal Link Scheduling in Millimeter Wave Multi-hop Networks with MU-MIMO radios." *Accepted in IEEE Transactions on Wireless Communications*, 2020.

[13] M. Rebato, M. Mezzavilla, S. Rangan, F. Boccardi, and M. Zorzi, "Understanding noise and interference regimes in 5G millimeter-wave cellular networks," in *22th European Wireless Conference*, May 2016, pp. 1–5.

[14] E. Aarts, J. Korst, and W. Michiels, "Simulated annealing," in *Search Methodologies*. Springer, 2005, pp. 187–210.